LIU Zhengjiang, CHO Hiroshi, MA Lina, et al. Numerical study of surface water flooding characteristics in urban environments [J]. Water Resources and Hydropower Engineering, 2025, 56(10): 46-57. DOI: 10.13928/j.cnki.wrahe.2025.10.004
刘正疆, 张浩, 马丽娜, 等. 城市地表雨洪特征的数值模拟研究[J]. 水利水电技术(中英文), 2025, 56(10): 46-57. DOI: 10.13928/j.cnki.wrahe.2025.10.004

Numerical study of surface water flooding characteristics in urban environments

LIU Zhengjiang[1], CHO Hiroshi[2], MA Lina[3], LIANG Dongfang[4]

(1. GeoLogical Survey of Gansu Province, Lanzhou 730000, Gansu, China; 2. Faculty of Engineering, Kumamoto University, Kumamoto 860-8555, Japan; 3. School of Civil Engineering, Lanzhou Jiaotong University, Lanzhou 730070, Gansu, China; 4. Department of Engineering, University of Cambridge, Cambridge CB2 1PZ, UK)

Abstract: [Objective] Surface water flooding is caused by heavy rainfall, which has been the main type of flooding in many cities across the world. Real urban environments are highly complex, and there are numerous parameters influencing the rainfall-runoff processes, such as road width, orientation and building coverage. The main objective is to perform a parametric study concerning the rainfall-runoff processes in complex urban environments, in order to gain a better understanding of the impact of urban characteristics on the surface runoff. [Methods] Realistic urban layouts are generated by means of procedural modelling software, which parameterises the urban configurations using 11 independent variables, including the averaged street length, street orientation, street curvature, major street width, minor street width, park coverage, etc. A shock-capturing TVD MacCormack shallow water equations solver is used to undertake a large number of computational simulations regarding the rainfall-runoff processes over realistic urban layouts. The dominating urban parameters that influence the time of concentration is unveiled, which characterises the timescale of the flood formation. [Results] In order to generalise the research outcomes, the obtained hydrographs at the outlet of the catchment are normalised so that they are independent of the catchment area, slope or rainfall intensity. The dimensionless time of concentration is thus only the functions of 12 independent parameters, including 11 parameters that governing the urban layouts and the Manning roughness coefficient of the ground. A sensitivity analysis, based on the multiple linear regression method, is performed on the 2,994 simulation cases to quantify the influence of each parameter. [Conclusion] The results show that the ground roughness and the building coverage ratio are the two most important factors that influence the urban flood formation. Their influences on the dimensionless timescale of the urban catchments' response to rainfall are quantified by empirical formulae. The research findings can provide useful guidelines for the design of future flood-resilient urban environments and the improvement of existing drainage systems in cities.

Keywords: urban flooding; surface water flooding; shallow water equation; time of concentration; rainfall-runoff; flood forecasting; precipitation; human activity

DOI: 10.13928/j.cnki.wrahe.2025.10.004 开放科学(资源服务)标志码(OSID):

中图分类号: TV122+.1 **文献标志码**: A **文章编号**: 1000-0860(2025)10-0046-12

Article history: Received 10 January 2025; Revised 18 January 2025; Accepted 20 January 2025; Available online 14 February 2025

收稿日期: 2025-01-10; **修回日期**: 2025-01-18; **录用日期**: 2025-01-20; **网络出版日期**: 2025-02-14

Financial Aid: Technology Research and Development Program, Department of Natural Resources of Gansu Province (2023-2-08); The Engineering and Physical Sciences Research Council (EP/N021614/1)

基金项目: 甘肃省自然资源厅科技开发计划项目(2023-02-08); 英国工程和自然科学研究委员会(EP/N021614/1)

About the author: LIU Zhengjiang (1994—), male, engineer, project team leader, master degree, mainly specialized on geological disaster survey, assessment and mitigation. E-mail: 673172339@qq.com

作者简介: 刘正疆(1994—), 男, 工程师, 项目组组长, 硕士, 主要从事地质灾害调查评价与防治研究工作。E-mail: 673172339@qq.com

Corresponding author: MA Lina (1985—), female, associate professor, project team leader, doctor, mainly engaged in theoretical studies on geotechnical properties of special strata. E-mail: 276153631@qq.com

LIANG Dongfang (1975—), male, professor, research group leader, doctor, mainly engaged in hydraulic and hydro-environmental research. E-mail: dl359@cam.ac.uk

通信作者: 马丽娜(1985—), 女, 副教授, 项目组组长, 博士, 主要从事特殊地层特性及理论研究工作。E-mail: 276153631@qq.com

梁东方(1975—), 男, 教授, 研究团队负责人, 博士, 主要从事水力学和水环境研究。E-mail: dl359@cam.ac.uk

城市地表雨洪特征的数值模拟研究

刘正疆[1]，张　浩[2]，马丽娜[3]，梁东方[4]

(1. 甘肃省地质调查院，甘肃 兰州　730000；2. 熊本大学 工学部，日本 熊本　860-8555；3. 兰州交通大学 土木工程学院，甘肃 兰州　730070；4. 剑桥大学 工程系，英国 剑桥　CB2 1PZ)

摘　要：【目的】局部强降雨引发的地表洪水已经成为很多城市洪水的主要形式。真实的城市环境非常复杂，影响地表降雨-产流的因素很多，比如马路宽度、方向和建筑物覆盖率。通过开展大量不同参数组合的数值模拟试验，得到城市地表特征对降雨-产流过程的影响。【方法】具有真实感的地表形态是采用程序化建模软件自动生成的。这款软件通过11个独立参数描述城市地表形态，包括平均街道长度、街道方向、街道曲率、主路宽度、辅路宽度、公园覆盖率等。研究采用具有激波捕捉功能的总变差减少的麦科马克格式求解浅水方程组，得到了大量不同城市地表的降雨-产流过程。研究揭示了影响城市雨洪汇流时间的主要参数。这个汇流时间代表了洪水形成的特征时间尺度。【结果】为了得到普遍适用的结果，研究将计算得到的流域出口的流量过程线归一化，使之不受流域面积、坡度和雨强的影响。因此，无量纲汇流时间取决于12个独立参数，即11个控制城市地表形态的参数和第12个描述地面粗糙程度的曼宁系数。基于多元线性回归的方法，对2 994个数值模拟的结果进行了敏感性分析，定量研究了每个参数对计算结果的影响。【结论】结果表明：地表粗糙度和建筑物覆盖率是影响城市雨洪形成的最主要的两个参数。提出的经验公式描述了各参数对流域无量纲汇流时间的影响。研究成果可以为未来设计具有韧性防洪能力的城市环境和改进现有的排洪系统提供有益的指导。

关键词：城市洪水；地表洪水；浅水方程；汇流时间；降雨产流过程；洪水预报；降水；人类活动

1　Introduction

In contrast to plenty of studies on fluvial flooding, both experimentally and numerically, there have been limited researches on the influence of buildings on the catchments' response to intensive rainfalls. However, short-lived storms often cause severe damages in city environments. Deadly pluvial floods are becoming more and more frequent, causing substantial damage in densely populated areas. Changing precipitation patterns, ageing drainage infrastructure and rapid urbanisation all demand for a better understanding of rainfall-runoff processes and the design of flood-proof urban systems. There have been numerous studies on the rainfall-runoff over simplified slopes[1-6] and on pluvial flooding in idealized or specific urban setups[7-13]. Research on the diffuse pollutant transport has also been increasingly reported in idealized situations[14-16]. However, it is difficult for these results to be generalised and there is little research on how different urban characteristics affect flooding. Urban environments are highly complex and it is likely that the flow due to rainfall is affected by numerous urban parameters, e. g. urban characteristics such as road width, orientation or building coverage. BRUWIER et al.[17] investigated the respective influence of various urban pattern characteristics on fluvial inundation flows. A set of 2, 290 synthetic urban patterns were generated using an urban procedural model that provided locations and shapes of streets and buildings over a square domain of one by one square kilometers. No such study has been conducted concerning the rainfall-runoff processes.

In recent years, more and more physically-based hydrodynamic methods have been proposed, as opposed to the conceptual hydrological methods. Because the surface runoff is often confined in a thin layer with large horizontal extents, the fully-dynamic shallow water

equations (SWEs) are able to model these flows accurately. In the context of rainfall-runoff studies, ZHANG and CUNDY[18] are among the first who solved the two-dimensional (2D) fully-dynamic SWEs numerically and found the importance of ground micro-topography to the overland flow process. In recent years, there has been an increasing trend of extending the application of the SWEs to the catchment-scale and urban hydrological studies[19-20]. In order to save the computational cost, various simplifications to the fully dynamic SWEs have been more commonly used in the past, including the kinematic wave and diffusive wave models[21-24]. The diffusive wave model neglects the inertia of the fluid in the momentum equations, while the kinematic wave model further neglects the effect of pressure gradient on the water motion. Lots of studies can be found concerning their applicability in various conditions[25-26]. However, rapidly varying flows due to sudden changes in topography cannot be handled properly by these simplified models[27].

This paper uses a Total Variation Diminishing (TVD) MacCormack numerical scheme to solve two-dimensional SWEs. First, the model was validated against published data. Steady water depths in BRUWIET et al.[17] were reproduced when applying a steady inflow of water through computer-generated building arrays, confirming the capability of the present model in simulating prescribed water flow over near-realistic urban layouts. Next, the rainfall-runoff processes over hundreds of computer-generated near-realistic urban layouts were simulated. With the combination of various unceasing rainfall intensities and ground slopes, a total of 2, 994 hydrographs, i. e. S-curves, at the catchment outlet were recorded. To generalise the research outcomes, the dimensional analysis was exploited in the examination of S-curve normalisation method. The dimensionless S-curves are only dependent on the urban layouts, rather than the rainfall intensity or ground slope. This allowed for the use of a dimensionless time of concentration to characterise the time-scale of the catchment response. Finally, a multiple linear regression model was used to the sensitivity of catchment response to twelve urban parameters. The most influential factors were found to be Manning roughness coefficient and building coverage, followed by the street length, building side setback, parcel area and to a lesser extent, street orientation and curvature. The time scale of the hydrological response is reduced with the reduction of the Manning roughness coefficient and with the reduction of the building coverage.

2 Model Setup

2.1 SWEs and solver

The 2D SWEs are a set of partial differential equations, derived based on the principle of conservation of mass and momentum in two horizontal directions. They describe the evolution of incompressible flow in response to gravity, bed friction and inertia. Neglecting Coriolis, wind and viscous forces, the SWEs take the following form in the Cartesian systems. The formulas are as follows

$$\frac{\partial \eta}{\partial t} + \frac{\partial q_x}{\partial x} + \frac{\partial q_y}{\partial y} = i \tag{1}$$

$$\frac{\partial q_x}{\partial t} + \frac{\partial (q_x{}^2/H)}{\partial x} + \frac{\partial (q_x q_y/H)}{\partial y} = -gH\frac{\partial \eta}{\partial x} - \frac{n^2 g q_x \sqrt{q_x{}^2 + q_y{}^2}}{H^{7/3}} \tag{2}$$

$$\frac{\partial q_y}{\partial t} + \frac{\partial (q_x q_y/H)}{\partial x} + \frac{\partial (q_y{}^2/H)}{\partial y} = -gH\frac{\partial \eta}{\partial y} - \frac{n^2 g q_y \sqrt{q_x{}^2 + q_y{}^2}}{H^{7/3}} \tag{3}$$

where t is time, s; x and y are the two horizontal Cartesian coordinates, m; η is the water surface elevation, m; q_x and q_y are the volumetric discharges per unit width in the x and y directions, respectively, $m^2 \cdot s^{-1}$; n is the Manning's roughness coefficient, $m^{-1/3} \cdot s$; H is the total water column depth, m; g is the acceleration due to gravity, $m \cdot s^{-2}$; i is the rainfall intensity, which is equal to the flow rate per unit plan-surface area, $m \cdot s^{-1}$.

For the numerical solution of these coupled partial differential equations, a TVD MacCormack finite difference numerical scheme is applied. This scheme was first proposed for supersonic compressible flows and is capable of solving the non-linear SWEs at a high efficiency and has been extensively validated against published experimental and analytical results. Detailed implementation of the numerical scheme and details of the

numerous validation tests can be found in LIANG et al[9-28].

In order to represent buildings or obstacles, the building-hole method was used, where the grid cells representing buildings are excluded from the computation. The elevations of these grid cells are increased in order to prevent any flow of water into these 'holes'. The rainfall intensity over the whole domain was increased to compensate for the 'loss' of rainfall falling over these 'holes'[7-8].

2.2 Urban patterns

The first stage of the study is focused in the generation of realistic urban layouts. BRUWIER et al.[17] examined hydraulic computations on 2, 290 urban configurations using an anisotropic porosity model. Urban configurations were generated by means of a self-developed urban generator tool, based on a procedural modelling technique developed at Purdue University by the team of Prof. Daniel G. ALIAGA. The building geometries and locations were controlled using 11 urban parameters, as listed in Table 1. Each of the parameters was randomly selected from a range of variation, representative of the real-world condition of built environments. The urban layouts were obtained in a shapefile format and were subsequently converted to the format compatible with the model used in the TVC MacCormack solver.

Table 1 Ranges of the 11 parameters used in urban generator

表 1 城市地表形态生成的 11 个参数范围

ID	Parameter	Minimum value(P_{min})	Maximum value(P_{max})
P1	Average street length/m	40	400
P2	Street orientation/(°)	0	180
P3	Street curvature/rad	0	0.42
P4	Major street width/m	16	33
P5	Minor street width/m	8	16
P6	Park coverage/%	5	40
P7	Maximum parcel area/m^2	300	1 100
P8	Building front setback/m	0	5
P9	Building rear setback/m	0	5
P10	Building side setback/m	0	5
P11	Building coverage/%	0	42.8

2.3 Model verification

BRUWIER et al.[17] are among the first to perform a parametric study on computer-generated near-realistic urban configurations. Using an anisotropic porous model, they investigated the influence of several urban pattern characteristics on inundation depths along the upstream boundaries. An example urban layout is illustrated in Fig. 1, with the grey blocks representing buildings. A steady inflow of water was prescribed at the inlet of the catchment, shown by red vectors at the bottom left of the example domain in Fig. 1, while a constant water depth was specified at the outlet, shown by the blue line at the top right of the example domain in Fig. 1.

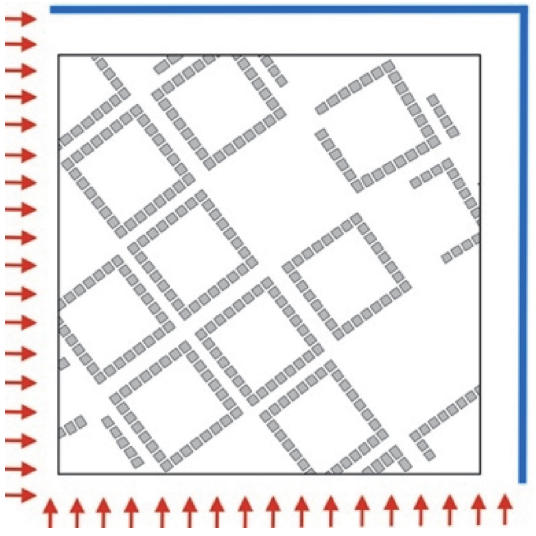

Fig. 1 A plan view of the urban layout and boundary conditions in BRUWIER et al.[17]

图 1 BRUWIER et al.[17]使用的城市地表形态俯视图和计算边界条件

The ground slope is zero in this verification case. The value of the Manning roughness coefficient was set to 0.04 $m^{-1/3} \cdot s$, which is comparable to the values suggested in previous studies. A steady inflow of 200 $m^3 \cdot s^{-1}$ prescribed along the upstream boundary at the left bottom. The specific discharge across the downstream boundary was specified according to the following rating curve function

$$q_j = C_1 \Delta \sqrt{2g(H_j - C_2)^3} \quad (4)$$

where sub-index j indicates the value at grid cell j; Δx is grid spacing, m; the constants are $C_1 = 0.5$ and $C_2 = 0.3$; and H_j is the computed water depth in cell j, m.

With a resolution of 1 m × 1 m computational grid cells, which means that 1 million grid cells were deployed over the whole computational domain, converged and stable results were obtained. Visualisation of the steady

state depths (colour contours) and velocities (vector arrows) is shown in Fig. 2(a, b, c) for three building configurations A, B and C, with buildings shown in white. Only every twentieth vector is plotted to illustrate the field fields. It is seen that the flow through the narrow gaps between buildings is well resolved. As the overall flow is diagonally towards the upper right, consistent water depth drop can be observed in that direction.

The flow of water across the lower left corner in configuration A, shown in Fig. 2(a), is obstructed by the block of buildings, resulting in considerably large water depths reaching more than 1.15 m. A more advantageous street and building orientation in Fig. 2(b) can reduce the inundation depths significantly. The dispersion of buildings across the domain allows easy flow of flood water towards the downstream boundaries and lower water depths as a result. In order to compare simulation results for different configurations, BRUWIER et al.[17] used h_{90}, the 90th percentile of water depths in each cell of the upstream boundaries. A similar approach was followed in this study and water depths along the upstream boundary (starting from top left to bottom right of the domain) were initially plotted, shown in Fig. 3. Subsequently, h_{90} was calculated for the three curves and compared with the porous model results obtained in BRUWIER et al.[17], with a maximum difference of around 0.15 m. The reasonably close agreement between the two different models of different resolutions manifests that the current predictions are reliable. A large number of verification cases have also been reported in LIANG et al.[9], confirming the capability of the TVD MacCormack model.

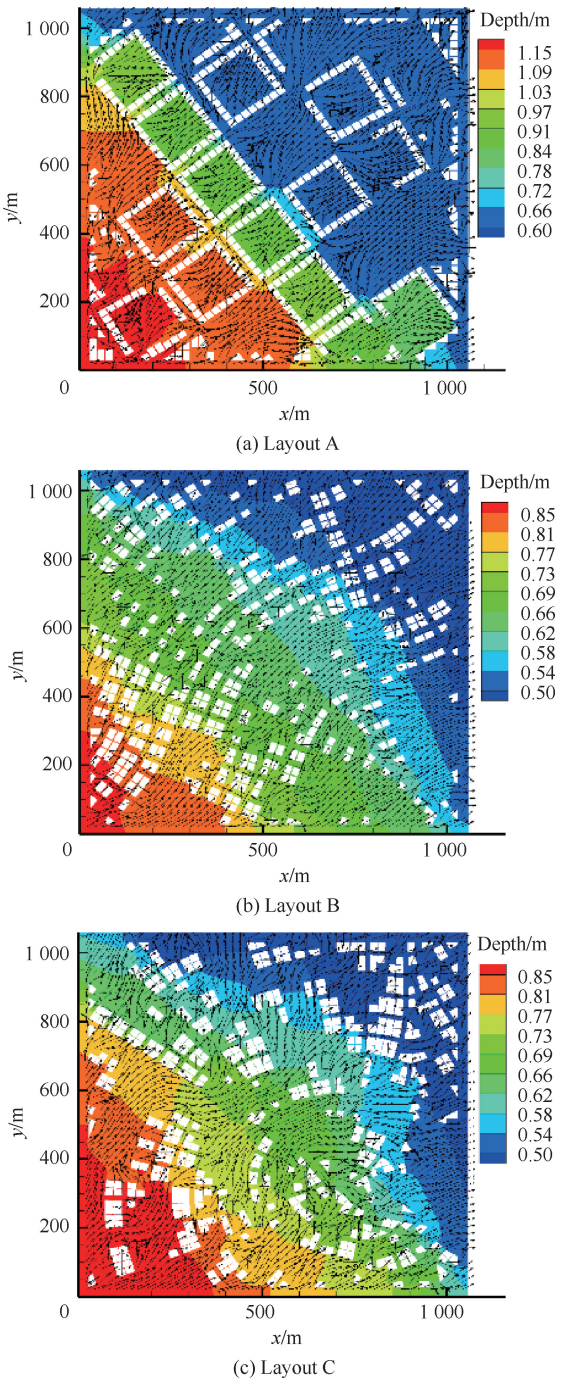

Fig. 2 Reproduction of the steady flow fields in BRUWIER et al.[17]

图 2 重现 BRUWIER et al.[17]得到的稳态流场

3 Hydrological Analysis

3.1 Normalised S-curve and time of concentration

If continuous rainfall of intensity i falls uniformly over an impervious area A, the discharge from the basin outlet will rise and, after a period, reach equilibrium. This is when the volumetric outflow rate equates the volumetric rate of rainwater introduced to the catchment. The resulting steady outflow rate Q will then be equal to iA. The hydrograph at the catchment outlet produced by unceasing uniform rainfall of constant intensity is referred to as the S-curve. The time to reach the equilibrium is known as 'the time of concentration', roughly equal to the time taken for the raindrop falling on the furthest part of the catchment to reach the outlet.

The hydrological response of the catchment will then be dependent on the following independent variables: rainfall intensity, size and slope of the catchment, ground roughness and building layout in the catchment. In this study, the slope of the catchment is specified in the x

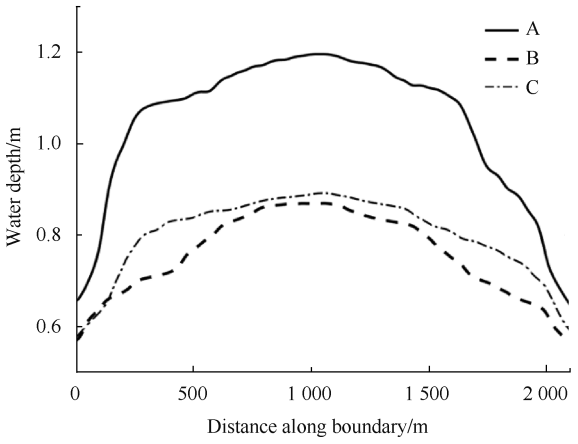

Fig. 3 Water depth variation along the upstream boundary

图 3 沿上游边界的水深变化曲线

axis, so the overall flow is along the positive x direction. The wall boundary condition is set along the left, top and bottom of the domain, while the critical flow condition is specified at the outlet of the domain on the right. A number of simulations were first conducted by changing the uniform unceasing rainfall intensity and the catchment slope, while other catchment variables were fixed. The obtained hydrographs at the catchment outlet, i. e. S-curve, are obtained by integrating q_x across right boundary of the domain and plotted in Fig. 4. As expected, significant differences in the time of concentration and steady outflow rate arise from the different combinations of rainfall intensity i and slope S. In order to enable the development of an approach that compares hydrological response based on the characteristics of the built environment, independent of the above parameters, we follow a dimensionless hydrograph approach.

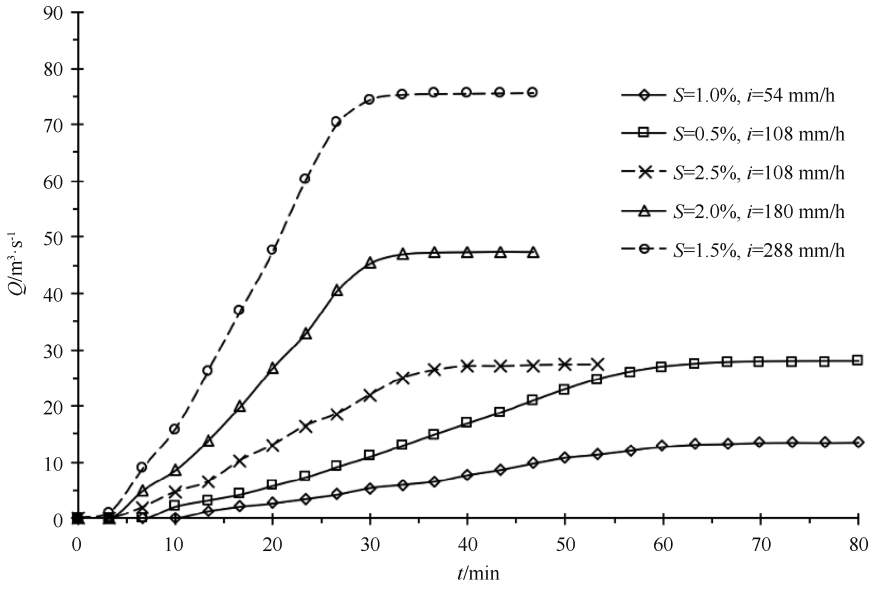

Fig. 4 S-curves with different rainfall intensities and catchment slopes

图 4 不同降雨强度和流域坡度条件下的 S-曲线

Following a similar approach to LIANG et al.[9], the dimensionless time and the dimensionless flow rate are considered for this analysis. The formula is as follows

$$Q^* = \frac{Q}{i \times A} \tag{5}$$

The dimensionless flow rate chosen is simply the ratio between the outflow rate Q and the volumetric rate of rainwater falling on the catchment iA, which ranges from 0 to 1. The dimensionless time is shown in Eq. (6), encompassing time t, domain slope S, gravitational acceleration g and domain area A. The formula is as follows

$$t^* = \frac{t \times \sqrt{S \times g}}{A^{0.25}} \tag{6}$$

The resulting dimensionless hydrographs are shown in Fig. 5. The dimensionless hydrographs under different combinations of catchment slope and rainfall intensity are seen to collapse to a single curve. The S-curves are closer in the rising and equilibrium portions of the hydrographs.

The time of concentration characterises the hydrological response of the catchment[29-30]. While this concept is theoretically sound, it is impractical to use in real simulations. S-curves generally reach the equilibrium state at a very low rate, also witnessed in Fig. 4-5. Estimation of the full time of concentration would therefore result in large errors and is undesirable. It is common for researchers to use t_{25}^* or t_{50}^*, the times to reach 25% or 50% of equilibrium flow rate, respectively. However, LAM[31] showed there is additional benefit of having a bigger variation of dimensionless time, t_{70}^*, when comparing dimensionless hydrographs of building configurations. Therefore, time to reach 70% of the dimensionless equilibrium flow rate, t_{70}^*, will be used in the next session to characterise the rainfall-runoff response.

Fig. 6 shows the flow fields of three

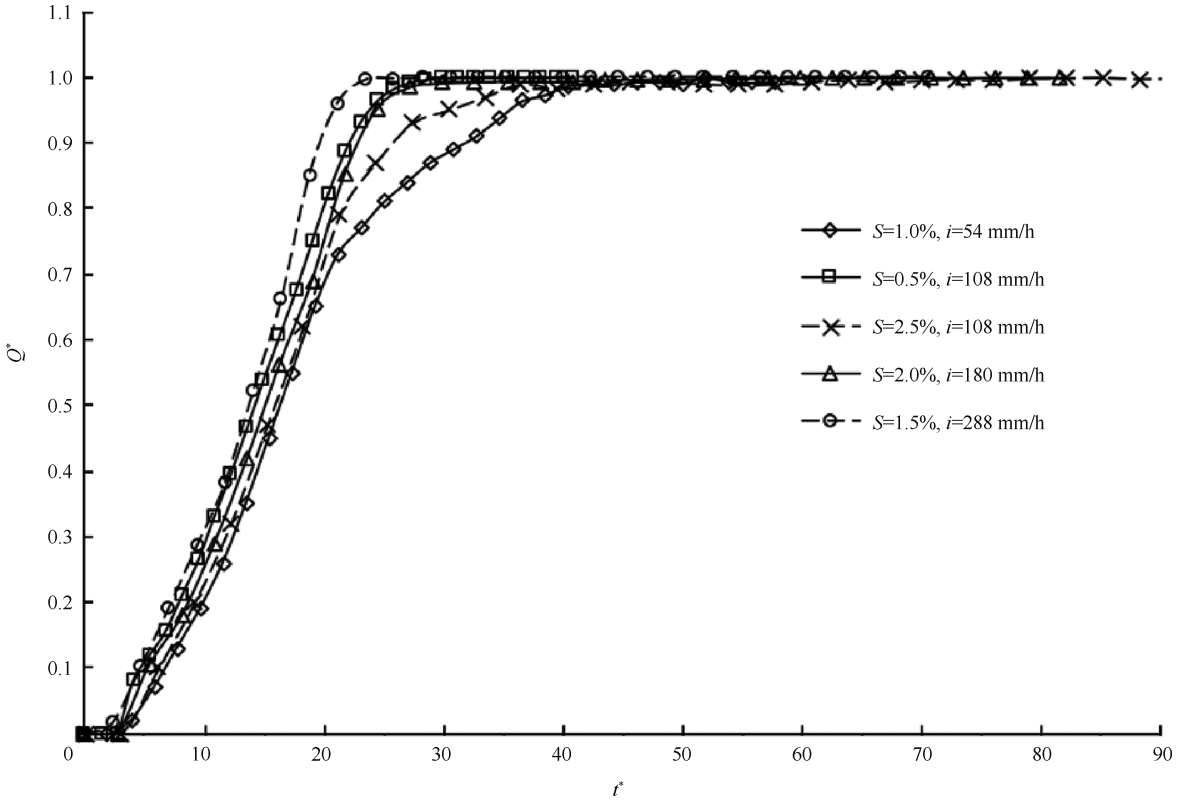

Fig. 5 Dimensionless S-curves with different rainfall intensities and catchment slopes

图 5 不同降雨强度和流域坡度条件下的无量纲 S-曲线

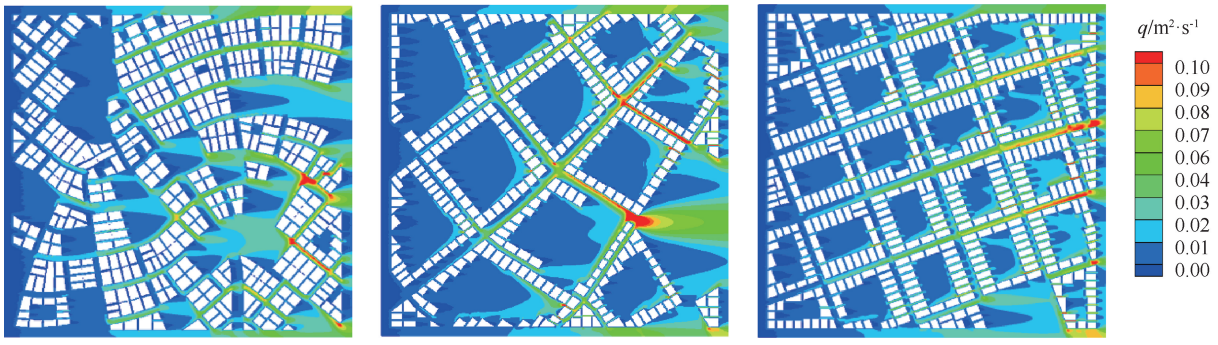

Fig. 6 Magnitude of the unit-width flow rates for three example urban layouts

图 6 绕三个典型城市建筑群的单宽流量分布

urban layouts at the equilibrium stage, with buildings represented by white colour. The corresponding urban layout parameters and values of t_{70}^* are listed in Table 2, when the Manning's roughness coefficient is 0.04 $m^{-1/3} \cdot s$. In layout A, the low average street length (P1) allows for a better flow distribution around the domain. In layouts B and C, areas surrounded by buildings display low flow velocities, suggesting their negligible contribution to the overall flow. Flow is instead intensified along the streets, shown by the considerably

Table 2 Three urban layout parameters and the corresponding values of t_{70}^* (n = 0.04 $m^{-1/3} \cdot s$)

表 2 三个典型城市形态参数及其对应的 t_{70}^*数值(n = 0.04 $m^{-1/3} \cdot s$)

Layout	P1/m	P2/(°)	P3/rad	P4/m	P5/m	P6/%	P7/m^2	P8/m	P9/m	P10/m	P11/%	t_{70}^*
A	100.5	57.3	0.341	29.9	12.4	26.3	1073	1.0	1.1	2.8	37.2	26.5
B	295.0	155.1	0.287	28.5	10.3	23.7	898	1.1	3.0	3.0	23.2	28.9
C	212.3	24.0	0.051	20.7	12.8	10.4	810	1.1	1.9	3.1	34.4	27.1

higher flow velocities.

3.2 Multivariable regression

A sensitivity analysis was undertaken to identify the influence of various urban parameters on rainfall-runoff processes. Use of High Performance Computing (HPC) and parallel processing enabled the simulation of 2, 994 rainfall-runoff processes on 998 different urban layouts. The dependence of t_{70}^* on a number of urban characteristic was then quantified using a Multiple Linear Regression (MLR) algorithm, allowing the identification of the most influential urban parameters.

Section 2.1 mentioned 11 independent parameters for defining the building layouts. In addition to these, the Manning roughness coefficient can also influence the nondimensional rainfall-runoff relationship. Hence, this paper examines the influence of 12 parameters on urban runoff. The ranges of the 11 parameters are given in Table 1, while three values of the Manning roughness coefficient were tried: 0.02, 0.04 and 0.07 $m^{-1/3} \cdot s$.

The MLR enables the study of each parameter's influence separately by isolating its role from all the others. The relationship between each influencing parameter and t_{70}^* is determined from a linear approximation that best approximates the data points. This approach yields 12 regression coefficients (β_1, β_2 …, β_{12}), each representing the mean change in the value of t_{70}^* for one unit change in each influencing parameter, while holding other parameters constant. In order to perform MLR, it is important to transform the 12 parameters and t_{70}^* into non-dimensional, scale invariant variables. Standardisation of a variable was easily achieved by subtracting the population mean from this variable and then dividing by the standard deviation of the population, with the size of population being 2, 994.

Table 3 and Fig. 7 show the 12 coefficients β_i ($i=1$, …, 12) obtained from the regression analysis, representing the sensitivity factors on the dependent variable t_{70}^*. Positive coefficients indicate a positive correlation between the relevant parameters and t_{70}^* and contrariwise for negative values. The ratio between each coefficient β_i and the largest coefficient β_{max} was also calculated to reveal the relative differences between the sensitivities of parameters.

Table 3 Regression coefficients for 12 independent parameters

表 3 12 个独立参数的回归系数

ID	Parameters	β_i	β_i/β_{max}/%
P1	Street length	0.062 3	6.7
P2	Street orientation	0.012 7	1.4
P3	Street curvature	0.012 3	1.3
P4	Street width (major)	−0.006 4	−0.7
P5	Street width (minor)	−0.002 9	−0.3
P6	Park coverage	−0.011 1	−1.2
P7	Parcel area	−0.047 1	−5.0
P8	Front setback	−0.011 7	−1.3
P9	Rear setback	0.016 5	1.8
P10	Side setback	−0.042 7	−4.6
P11	Building coverage	0.316 0	33.8
P12	Roughness n	0.934 6	100.0

Overall, it can be concluded that the MLR model used is very reliable, as evidenced by a zero associated p-value and a close-to-unity value of $R^2 = 0.96$. A zero p-value indicates that the model, consisting of 12 independent variables, can reliably predict the dependent variable. In order to consider the reliability of each coefficient β_i to predict non-dimensional t_{70}^*, the p-value

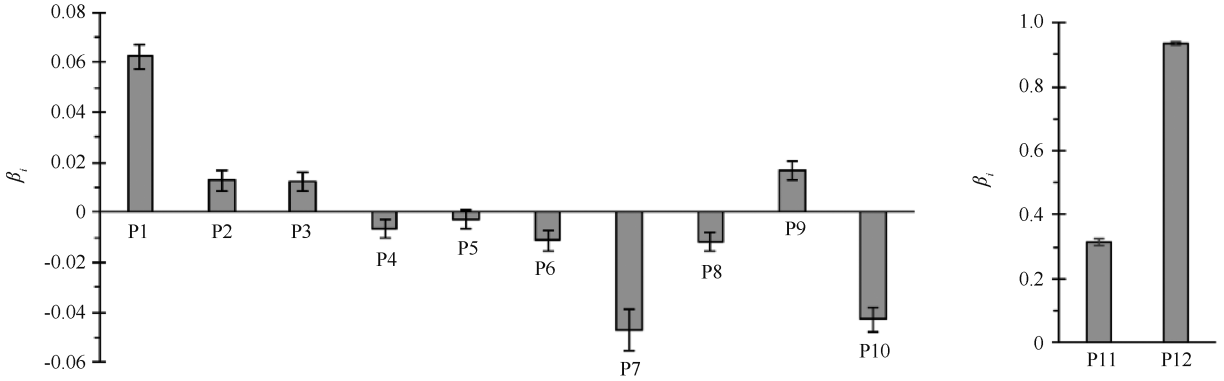

Fig. 7 Graphical representation of 12 regression coefficients

图 7 12 个拟合参数的柱状图

for each coefficient was found to be less than 0.05, meaning that the null hypothesis can be rejected and the coefficient is statistically significant. Regarding R^2, a value of 0.96 indicates that 96% of the variance in the dependent variable can be predicted from the independent variables, again confirming the reliability of the model.

As seen from Table 3 and Fig. 7, the most influential parameter is the ground roughness n (P12), followed by Building Coverage (P11). These two are many times more influential than the other parameters, which is why they were plotted in a separate scale in Fig. 7. The large influence of roughness indicates that the shallow runoff is largely governed by microscale topography, rather than macroscale characteristics such as P1-P11. Building coverage is the second most influential parameter, as water should flow around buildings in the domain. Although it could be argued that an advantageous street network in a dense urban environment could in theory ease the flow of water through the city, such a preferential flow path is unlikely to exist in randomly generated urban layouts. The same can be said for real-life urban environments which are designed and developed in a 'random' fashion.

Street length (P1), which represents the average length of the streets present in the layout, also shows a significant effect on the catchment response. One plausible explanation is the influence this parameter has on the overall geometry of the layout. Longer streets imply larger clusters of buildings, making the layout less porous, which in turn reduces the number of available flow paths. As a result, water finds it difficult to penetrate the building clusters, hence a longer time to leave the urban area. A similar argument can be made for building side setback P10; greater side gaps between buildings increase the number of available flow paths, hence the negative relationship with dimensionless time.

Parcel area (P7) is a measure of the area belonging to a single building. It could be argued that, generally, a large parcel area implies more space around individual buildings for water to flow about. This would result in more potential flow paths and therefore lower the time of concentration. A large value of the front building setback (P8) has an effect of 'widening' the roads, hence the negative relation-ship with the time of concentration. In the contrary, rear setback (P9) shows a positive relationship. This could be explained by the fact that an increasing back-to-back gap between buildings (as rear setback is increased) promotes the accu-mulation of water in between building blocks, which tends to 'delay' the water flow.

The positive values for street orientation (P2) and curvature (P3) are related to how buildings 'guide' the flow of water. As expected, an increase in the curvature prevents the straight flow paths and thus slows down the flow. The effect of street orientation is affected by the direction of the slope. In our case, the slope is along the x-axis, which corresponds to a zero angle of orientation. Therefore, it is expected that an increasing angle of orientation increases the misalignment between the streets and the slope of the catchment, hence the positive relationship between P2 and dimensionless time of concentration.

The negative influence of the street width, both major (P4) and minor (P5), is as expected, as it is easier for water to move across an urban with wider streets. However, the correlation is very low, implying that water flow is influenced more by the street network, including connection and orientation, than by the street width.

3.3 Empirical relationships

The MLR model developed with 12 independent parameters displays good fit to the data, confirming the statistical significance. In order to identify patterns, relationships or anomalies among the data, it is important to visualise the results. The use of pairs plot, also known as a scatterplot matrix, enables visualisation of two-dimensional relationships between independent and standardised dependent variables. As expected, no visible relationship was observed for parameters P1-P10, as t_{70}^* is largely governed by n (P12) and building coverage (P11). Plotting t_{70}^* against these two parameters in Fig. 8-9 reveals the linear relationships as derived from the statistical analysis. The lines of best fit to the data points are also drawn. Although these relationships contain mixed information from other parameters P1-P10, it can be argued that P11-P12 play the dominant roles.

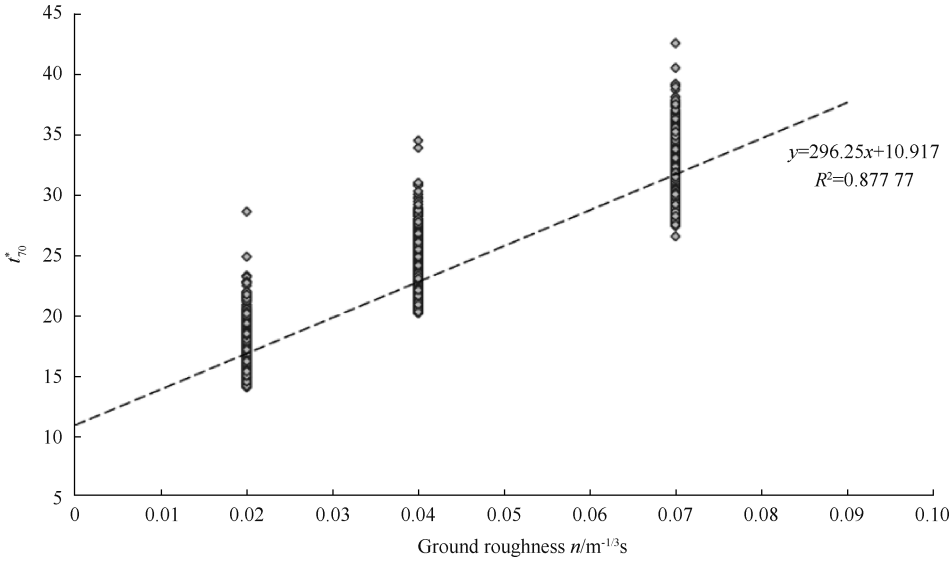

Fig. 8 Linear fit between t_{70}^* and Manning roughness coefficient

图 8 t_{70}^*和曼宁系数之间的线性拟合关系

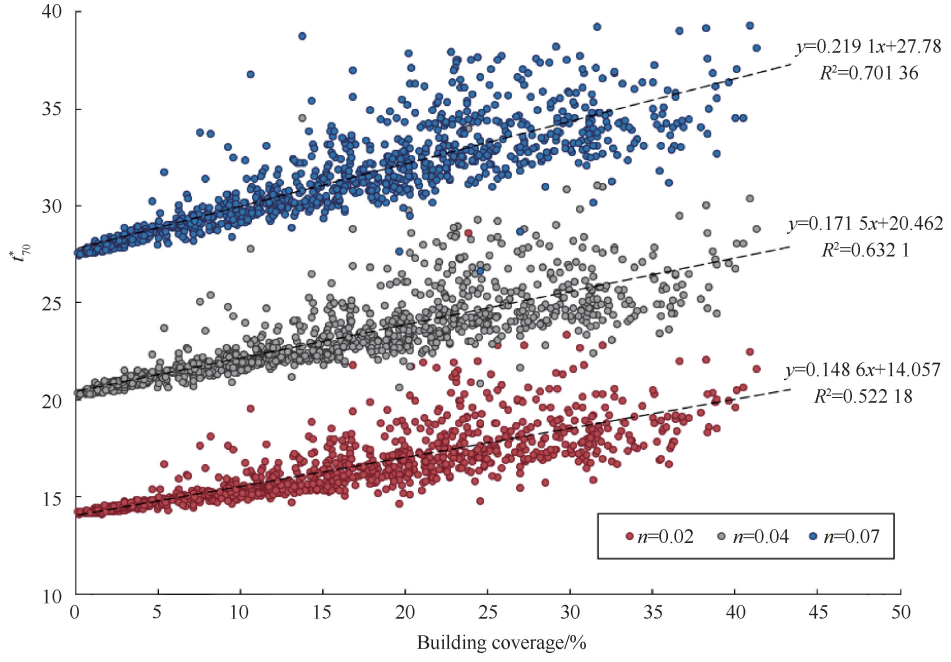

Fig. 9 Linear fit between t_{70}^* and building coverage

图 9 t_{70}^*和建筑覆盖率之间的线性拟合关系

From Fig. 9, it can be seen that the data points collapse to a distinct line at low building coverages and eventually a single point at zero building coverage. At this point, the domain is simply a sloping plane of roughness n without obstacles. The dimensionless time of concentration is thus simply governed by the roughness coefficient n. Increasing the building coverage, on the other hand, introduces additional variables affecting the flow. The influence of the other parameters (P1-P10) on dimensionless time of concentration is therefore increasing with a growing building coverage, shown by an increasing deviation of data points in Fig. 9. The data points belonging to different values of n are not as distinct as before, suggesting the growing influence of other parameters.

4 Conclusions

A high-resolution hydrodynamical model was applied

to study the rainfall-runoff processes over realistic urban layouts. General agreement with steady-inundation results in BRUWIER et al.[17] confirmed the accuracy of the model. Subject to unceasing unform rainfall, the study verified that the dimensionless S-curves are independent of the catchment size, slope and rainfall intensity, using a properly-constructed dimensionless time and dimensionless flow rate. Hence, the dimensionless S-curve is only a function of urban building characteristics and the ground roughness, allowing the use of a dimensionless time, t_{70}^{*}, to characterise the speed of the catchment response to rainfall.

High performance computing, parallel processing and automation enabled the simulation and processing of 2, 994 rainfall-runoff processes. Analysis of the results was achieved through the development of a reliable MLR model, which quantified the sensitivity of t_{70}^{*} to 12 urban characteristics. It was shown the most influential factors are Manning roughness coefficient and building coverage. Less influential parameters include street length, building side setback, parcel area and to a lesser extent, street orientation and curvature. Careful investigation of the relationships between t_{70}^{*} and the two most influential parameters, building coverage and roughness, unveils a decreasing influence of other urban characteristics at low building coverage. Empirical formulae were derived concerning the dependence of t_{70}^{*} on Manning roughness coefficient and building coverage.

Rainfall-runoff processes in urban environments are highly complex, as was shown to be influenced by multiple factors. This project decoupled these factors and quantified their influence on the hydrological response of urban areas, providing valuable knowledge on the influence of urban characteristics on rainfall-runoff processes. The study provides more insight on the design of future flood-resilient built environments.

5 Acknowledgements

We are grateful to the support by the Technology Research and Development Program, Department of Natural Resources of Gansu Province (Grant Number 2023-2-08) and the Engineering and Physical Sciences Research Council (Grant Number EP/N021614/1). The urban layouts were generated by a procedural model developed at Purdue University by the team of Prof. Daniel G. ALIAGA.

References:

[1] HENDERSON F, WOODING R. Overland flow and groundwater flow from a steady rainfall of finite duration[J]. Journal of Geophysical Research, 1964, 69(8): 1531-1540.

[2] SAÑUDO E, CEA L, PUERTAS J. Comparison of three different numerical implementations to model rainfall-runoff transformation on roofs[J]. Hydrological Processes, 2022, 36(5): e14588.

[3] SHAO F, WU J, TAO W, et al. A new analytical model for predicting overland flow and nutrient loss on hillslopes[J]. CATENA, 2022, 216(Part A): 106384.

[4] ZHANG J, LIU J T, HAN X L, et al. Variable storage behavior controlled by rainfall intensity and profile structure upon saturation excess overland flow generation[J]. Journal of Hydrology, 2022, 610: 127860.

[5] MORAWIECKI P, TRINH P H. On the development and analysis of coupled surface-subsurface models of catchments. Part 3. Analytical solutions and scaling laws[J]. Journal of Fluid Mechanics, 2024, 982: A30.

[6] JIN B M, YANG X, LEE K T, et al. Comprehensive interpretation of hillslope subsurface flow: An analytical approach to hillslopes with complex geometry[J]. Journal of Hydrology, 2025, 647: 132299.

[7] CEA L, GARRIDO M, PUERTAS J. Experimental validation of two-dimensional depth-averaged models for forecasting rainfall-runoff from precipitation data in urban areas[J]. Journal of Hydrology, 2010, 382: 88-102.

[8] SCHUBERT J E, SANDERS B F. Building treatments for urban flood inundation models and implications for predictive skill and modelling efficiency[J]. Advances in Water Resources, 2012, 41: 49-64.

[9] LIANG D, ÖZGEN I, HINKELMANN R, et al. Shallow water simulation of overland flows in idealised catchments[J]. Environmental Earth Sciences, 2015, 74(11): 7307-7318.

[10] MABROUK M, HAN H, FAN C, et al. Assessing the effectiveness of nature-based solutions-strengthened urban planning mechanisms in forming flood-resilient cities[J]. Journal of Environmental Management, 2023, 344: 118260.

[11] CIOFFI F, TIEGHI L, GIANNINI M, et al. Flash flood prediction in St. Lucia island through a surrogate hydraulic model[J]. Journal of Applied Water Engineering and Research, 2024, 12(3): 297-310.

[12] LIANG C, GUAN M F. Effects of urban drainage inlet layout on surface flood dynamics and discharge[J]. Journal of Hydrology, 2024, 632: 130890.

[13] PERRINI P, IACOBELLIS V, GIOIA A, et al. A tracer-aided 2D numerical framework to define fluvial and pluvial hazard mapping[J]. Journal of Flood Risk Management, 2025, 18(1): e13039.

[14] ZHANG T T, XIAO Y, LIANG D F, et al. A two-layer model for studying 2D dissolved pollutant runoff over impermeable surfaces[J]. Hydrological Processes, 2021, 35(5): e14152.

[15] XIAO Y, LUAN B, ZHANG T T, et al. Experimental study of sediment wash-off process over urban road and its dependence on particle size distribution[J]. Water Science and Technology, 2022, 86(10): 2732-2748.

[16] XIAO Y, ZHANG C, ZHANG T T, et al. Transport processes of dissolved and particulate nitrogen and phosphorus over urban road surface during rainfall runoff[J]. Science of The Total Environment, 2024, 948: 174905.

[17] BRUWIER M, MUSTAFA A, ALIAGA D G, et al. Influence of urban pattern on inundation flow in floodplains of lowland rivers[J]. Science of the Total Environment, 2018, 622/623: 446-458.

[18] ZHANG W, CUNDY T W. Modeling of two-dimensional overland flow [J]. Water Resources Research, 1989, 25(9): 2019-2035.

[19] MÜGLER C, PLANCHON O, PATIN J, et al. Comparison of roughness models to simulate overland flow and tracer transport experiments under simulated rainfall at plot scale[J]. Journal of Hydrology, 2011, 402: 25-40.

[20] SIMONS F, BUSSE T, HOU J, et al. A model for overland flow and associated processes within the Hydroinformatics Modelling System [J]. Journal of Hydroinformatics, 2014, 16(2): 375-391.

[21] FENG K, MOLZ G J. A 2-D diffusion-based, wetland flow model [J]. Journal of Hydrology, 1997, 196: 230-250.

[22] KAZEZYILMAZ-ALHAN C, MEDINA M A. Kinematic and diffusion waves: analytical and numerical solutions to overland and channel flow [J]. Journal of Hydraulic Engineering, 2007, 133(2): 217-228.

[23] GOTTARDI G, VENUTELLI M. An accurate time integration method for simplified overland flow models [J]. Advances in Water Resources, 2008, 31: 173-180.

[24] COSTABILE P, COSTANZO C, FERRARO D, et al. Is HEC-RAS 2D accurate enough for storm-event hazard assessment? Lessons learnt from a benchmarking study based on rain-on-grid modelling [J]. Journal of Hydrology, 2021, 603(Part B): 126962.

[25] MORAMARCO T, SINGH V P. Accuracy of kinematic wave and diffusion wave for spatial-varying rainfall excess over a plane[J]. Hydrological Processes, 2002, 16: 3419-3435.

[26] TSAI W C. Applicability of kinematic, noninertia, and quasi-steady dynamic wave models to unsteady flow routing [J]. Journal of Hydraulic Engineering, 2003, 129(8): 613-627.

[27] COSTABILE P, COSTANZO C, MACCHIONE F. Comparative analysis of overland flow models using finite volume schemes[J]. Journal of Hydroinformatics, 2012, 14(1): 122-135.

[28] LIANG D, LIN B, FALCONER R. Simulation of rapidly varying flow using an efficient TVD-MacCormack scheme[J]. International Journal for Numerical Methods in Fluids, 2007, 53(5): 811-826.

[29] BEVEN K J. A history of the concept of time of concentration[J]. Hydrology and Earth System Sciences, 2020, 24: 2655-2670.

[30] SIGNH V P. A note on the time of concentration[J]. Journal of Hydrologic Engineering, 2023, 28(12): 04023039.

[31] LAM P. Rainfall-runoff Processes in Urban Environments [D]. Cambridge: Department of Engineering, University of Cambridge, 2016.

(责任编辑　王海锋)